Desalination 457 (2019) 62–74

Contents lists available at ScienceDirect

Desalination

journal homepage: www.elsevier.com/locate/desal

Using feed-forward voltage-control to increase the ion removal rate during batch electrodialysis desalination of brackish water

Sahil R. Shah*, Sandra L. Walter, Amos G. Winter V

Department of Mechanical Engineering, Massachusetts Institute of Technology, Cambridge MA, USA

ARTICLE INFO

Keywords:
Electrodialysis
Control
Brackish
Batch
Production rate

ABSTRACT

Batch electrodialysis (ED) desalination, which relies on diluate recirculation to produce a desired product, is often conducted at constant voltage. Here we show that constant-voltage operation under-utilizes membrane area because the applied current is much lower than the limiting current early in a batch cycle. Time-variant voltage-control, targeted at raising the average ratio of applied to limiting current during a batch cycle, can therefore increase the rate of ion-transfer achievable using a fixed membrane area. We designed a feed-forward voltage controller, which provided within −15 to +20% of the desired current, and used it to raise the production rate by up to 37% ± 2%, relative to constant-voltage operation, without exceeding the limiting current density. Furthermore, an analytical prediction of the batch completion times was derived and validated under varying feeds (1500, 2000, and 3000 mg/L), products (200, 300, and 500 mg/L), and flow velocities (4.3, 6.4, and 8.5 cm/s). Supported by experiments, the predictive model indicates that time-variant voltage-control can provide the greatest increase in production rate at high feed-to-product concentration ratios and low flow velocities. This work will assist designers and operators seeking to size, evaluate, and maximize the production performance of new and existing batch ED processes.

1. Introduction

In recent years, the need for energy-efficient and high-recovery solutions for brackish water desalination has revived an interest in Electrodialysis (ED) technology [1-4]. An ED stack relies on the use of an electric field, across alternating cation (CEM) and anion exchange membranes (AEM) arranged in repeating cell-pairs, to draw ions from a desalinated diluate solution to a concentrated solution (Fig. 1). In industrial processes, a feed solution is continuously desalinated to a desired product concentration, within a single pass through one or more discrete ED stages (Fig. 2a). Where space is a constraining factor, the diluate is recirculated through a single ED stack several times to achieve the desired product concentration in a batch process (Fig. 2b) [5-8].

Several authors have investigated the cost-minimizing design of both continuous and batch processes [9-16], where the capital cost is primarily a function of the required membrane area. In these studies, the required membrane area is decreased by raising the current density *i*. This term represents the per unit-area flux of ions through an individual membrane. In continuous systems, this current density is maximized throughout the process length by applying different voltages *V* and numbers of cell-pairs *N* to the individual ED stages [12,17,18] (Fig. 2a). However, with batch desalination, most studies do not take the analogous approach of adjusting the stack voltage in a time-variant manner. Instead, the batch is often processed at a constant voltage [19-24]. Min and Kim performed constant-voltage desalination experiments and demonstrated that increasing voltage provided diminishing improvements in the salt removal rate [23]. Tanaka used simulation to identify the voltages and feed concentrations at which a constant-voltage batch ED process provides a lower energy consumption than reverse osmosis (RO) [20]. Nayar et al. [24] and Bian et al. [25] designed batch desalination systems for household and community-scale applications, respectively, but also limited their parameter-space to consider only constant-voltage operation.

Few authors have examined controlling the batch desalination process in a time-varying manner to reduce energy consumption and cost. Previously, we investigated the cost-optimal design of a constant-voltage, point-of-use ED system and discovered that raising the average current density using time-variant voltage actuation could cost [16]. Parulekar mathematically demonstrated that a time-variant voltage or current can yield a lower energetic cost than a constant-voltage process, when considering both pumping and desalination, but did not explore potential membrane area savings [26]. Leitz recommended controlling the batch process to maintain a constant ratio of current to diluate concentration, but did not justify his suggestion in detail, nor discuss the expected effect on batch time [27]. Rohman and Aziz investigated

* Corresponding author.
E-mail address: sahils@mit.edu (S.R. Shah).

https://doi.org/10.1016/j.desal.2019.01.022
Received 1 September 2018; Received in revised form 14 January 2019; Accepted 25 January 2019

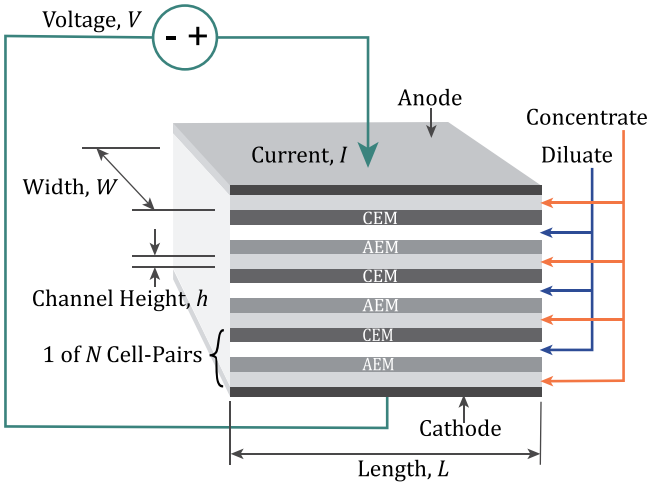

Fig. 1. In ED, an electric field is applied across alternating cation (CEM) and anion (AEM) exchange membranes to transport ions from the diluate channels to the concentrate channels. Diluate and concentrate outflows are omitted here for visual clarity.

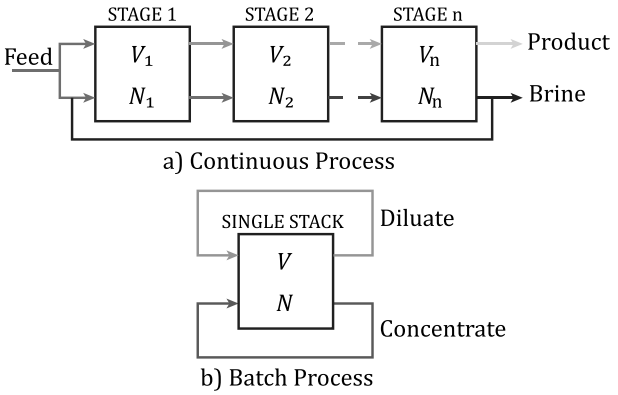

Fig. 2. (a) A saline feed is desalinated within a single pass through multiple ED stages in a *continuous process*, each with a different voltage V and number of cell-pairs N. (b) In a *batch process*, diluate is recirculated through a single ED stack until it is desalinated to a desired product concentration.

the optimal current density and flow rate, as a function of time, for several performance metrics related to a hydrochloric acid recovery process [13]. However, they did not implement a concentration-dependent limiting current density constraint in their simulations. Additionally, to our knowledge, the existing literature does not provide descriptions of batch ED controllers or experimental demonstrations of time-variant voltage-control.

Building upon this previous work, we sought to provide a comprehensive description, analysis, and experimental demonstration of time-variant voltage-control for batch ED desalination of brackish water. Specifically, we

1. detailed the concept and potential advantages of active voltage-control;
2. designed a bench-scale, feed-forward controller and experimentally implemented different voltage trajectories;
3. evaluated the decrease in batch duration, membrane usage, and energy consumption that can be safely achieved; and
4. derived a model to predict batch completion times, and validated it against voltage-controlled and constant-voltage tests.

While the use of time-variant voltage or current control is uncommon in ED, we acknowledge that it has been previously applied in other

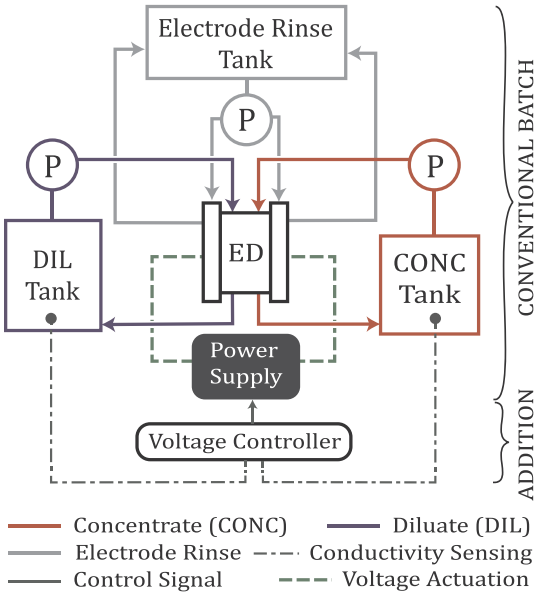

Fig. 3. Schematic of a conventional batch process. The addition of a controller allows voltage-controlled operation, based on conductivity measurements. "P" and "ED" represent the pump and ED stack, respectively.

electrochemical processes [28-31]. Most notably, Panizza et al. varied the stepwise current over time to increase the mineralization rate of organic pollutants on boron-doped diamond anodes in an electrolysis process, and lower energy consumption [32]. We therefore employ a similar approach in this work, adapting it to enhance batch ED.

2. The concept of active voltage-control

In batch ED desalination, an initial feedwater volume is separated at the desired recovery ratio into two circuits, one for the diluate and the other for the concentrate (Fig. 3). During desalination, the solutions are recirculated through the stack and a voltage is applied until the desired product concentration is obtained in the diluate tank. Both in simulation and practice, the voltage and recirculation flow rates are conventionally held constant during this process, as previously discussed. An additional third circuit may also be required to rinse the electrodes, but does not affect the following discussion.

The limiting current density is the concentration-dependent maximum salt removal rate that can be achieved before ions are depleted at the membrane surfaces. To avoid splitting water, affecting the product pH, and increasing the resistance to ion-transport, the ED stack is conventionally operated below this limiting current density. Assuming a short flow path and neglecting spatial concentration variations within the stack, the limiting current density i_{lim} [A/m^2] is plotted against the diluate concentration C_d^b, which only varies in time from the start to the end of one batch cycle (Fig. 4). When a constant voltage (CV) is applied, the corresponding current density trajectory is as shown for a sample scenario where a 2000 mg/L feed is desalinated to 100 mg/L. For this example, we require the instantaneous current density i [A/m^2] to be maintained below 90% of i_{lim}. This constraint only becomes active at the end of the constant-voltage batch process, when the diluate concentration has decreased to the desired product concentration C_{prod}. However, this point sets the maximum voltage that can be applied. Additionally, since the voltage is fixed, this point determines the current density trajectory for the full batch cycle. For earlier times in the cycle, the current density is much lower than limiting current density, causing the membranes to be under-utilized. The 'untapped capacity' represents the additional current that can be transmitted initially during the batch cycle, but remains unused with constant-voltage operation. This scenario is synonymous with continuous desalination

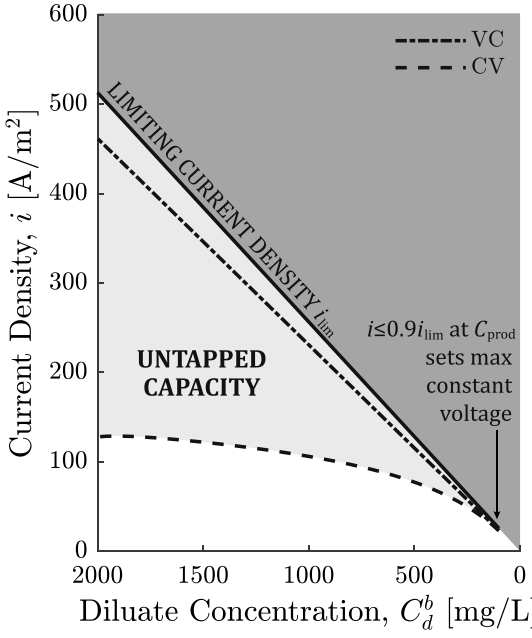

Fig. 4. Simulated current trajectories indicating the additional "untapped" desalination capacity captured with a voltage-controlled (VC) batch process over a constant-voltage (CV) batch. The bulk diluate concentration C_d^b is shown as decreasing in time along the x-axis, and the instantaneous current density i does not exceed 90% of the limiting current density i_{lim} for both cases.

using a series of ED stacks, but all at the same voltage which is determined by the limiting current density at the product concentration of the last stack.

Active voltage-control (VC) based on diluate conductivity measurements provides additional degrees of freedom to track (with an appropriate safety-margin) the limiting current density throughout the batch process (Fig. 4) and subsequently achieve higher ion-transfer rates. As a result, it can substantially increase the production rate of a system, or lower capital cost by decreasing the membrane-area required to satisfy a target production rate.

Measuring the diluate and concentrate conductivities is standard practice, and allows an operator to track the progress of a batch desalination process. The same data can be used to estimate the voltage for a desired current density (fully described in Section 4.2), thereby requiring no additional sensors for basic feed-forward control. The only addition required to implement voltage-control in this manner is a controller to administer an appropriate voltage to the ED stack based on conductivity measurements (Fig. 3).

3. Models

To maximize the current density i using feed-forward voltage-control, subject to $i < i_{lim}$, models for the limiting and applied current densities are required. The models applied below have been previously proposed and validated [19,33-35]. We additionally only consider the simple case of desalinating a sodium chloride solution in this study, which was found previously to provide reasonable estimates of the batch durations for real groundwater [34]. Lastly, although all concentrations are reported in more intuitive units of mg/L in this article, the following equations require concentrations expressed in units of mol/m^3.

3.1. Limiting current density

Assuming perfectly permselective ion-exchange membranes, the limiting current density is given as a function of the bulk diluate concentration C_d^b [mol/m^3] according to the modified Peers equation [36],

$$i_{lim} = \frac{C_d^b z F k}{1 - t^{+/-}}. \quad (1)$$

The charge number of either ion is $z = 1$ for sodium chloride, F is the Faraday constant 96,485, and $t^{+/-}$ is taken to be the minimum between the dimensionless anion and cation transport numbers in the bulk solution. The transport number represents the fraction of the total current carried by each ionic species.

Other theoretical and empirical expressions have been previously applied to model the limiting current density for solutions containing two [10,37], or more [38], ionic species. They can be used in place of Eq. (1). For these models, the limiting current density varies linearly with diluate concentration; therefore, the underlying parametric relationships derived in this work are not expected to change.

The boundary layer mass transfer coefficient k [m/s] is generally expressed in terms of the non-dimensional Sherwood number Sh,

$$Sh = \frac{k d_h}{D_{aq}}, \quad (2)$$

where D_{aq} [m^2/s] is the diffusion coefficient of the ions in the aqueous solution, and d_h [m] is the hydraulic diameter.

The Sherwood Number, which characterizes the mass-transfer, is correlated to the flow behavior and material properties of the diluate solution using an expression of the form

$$Sh = a Re^b Sc^c, \quad (3)$$

where the Reynolds Re and Schmidt Sc numbers are respectively defined as

$$Re = \frac{u_{ch} d_h}{\nu}, \quad \text{and} \quad (4)$$

$$Sc = \frac{\nu}{D_{aq}}, \quad (5)$$

with respect to the kinematic viscosity ν [m^2/s].

In this study, we use the coefficients $a = 0.29$, $b = 0.50$, and $c = 0.33$ based on the work of Pawlowski et al. [39]. These coefficients were previously [34] found to provide a good match with the limiting current density measurements on the same ED stack used in the following experiments (Section 4.1). This correlation relies on the following definitions of the hydraulic diameter d_h and linear flow velocity u_{ch} [m/s]:

$$d_h = \frac{4\epsilon}{2/h + (1 - \epsilon)(8/h)} \quad \text{and} \quad (6)$$

$$u_{ch} = \frac{Q}{\epsilon W h N}, \quad (7)$$

where h [m] is the thickness of the channel, W [m] is the width of the channel, Q [m^3/s] is the volumetric flow rate of diluate through the ED stack, N is the number of cell-pairs, and ϵ is the void fraction of the spacer occupying the channel.

Note that the diffusivity, transport numbers, and viscosity vary with sodium chloride concentration, but this dependence (Table 1) has a negligible effect on the limiting current density estimation for brackish water concentrations ($< \sim 3000$ mg/L). Therefore, they are treated as constants in this study. It follows then that once the flow rate through the ED stack is set, the limiting current density only varies linearly with the time-varying diluate concentration.

3.2. Applied current density

The objective of the proposed feed-forward voltage-control method is to maintain a desired instantaneous current density ratio r_i, defined as

$$r_i = \frac{i}{i_{lim}}. \quad (8)$$

Table 1
Transport properties and sensitivities to concentration and temperature.

Variable	Value	Variation	Ref
Transport numbers	$t^+ = 0.39$, $t^- = 0.61$	< 3% over 15–45 °C and 0–5000 mg/L	[40]
Diffusion coefficient, D_{aq}	1.6×10^{-9} m^2/s	< 8% over 0–5800 mg/L at 25 °C	[41]
Kinematic viscosity, ν	1×10^{-6} m^2/s	< 12% over 0–3000 mg/L at 20–25 °C	[42]

The voltage V [V] required to produce the desired current density i is

$$V = E_{el} + N[E_{mem} + i(R_d + R_c + R_{mem})], \tag{9}$$

where E_{el} is the potential drop of approximately 1.4 V due to redox reactions at the electrodes, E_{mem} [V] is the membrane potential, and R_{mem} [Ω-m^2] is the sum of the anion (AEM) and cation (CEM) exchange membrane resistances, respectively. An empirical model of R_{mem} for the experimental stack is provided in Appendix A. The resistances of the diluate and concentrate channels, respectively R_d and R_c [Ω-m^2], are related to the concentrations of the respective bulk flows, C_d^b and C_c^b, by

$$R_{d/c} = \frac{h}{\Lambda_C C_{d/c}^b}, \tag{10}$$

where the equivalent conductance Λ_C [S-m^2/mol] is a function of concentration and temperature (Fig. 5), and can be calculated using the Onsager/Falkenhagen equation with coefficients for NaCl [43]. During operation, conductivities ($\Lambda_C C^b$) are directly measured and used to compute the diluate and concentrate concentrations.

Under justified simplifications of equal diluate and concentrate channel flow rates and heights, perfectly permselective membranes, equal cation and anion transport numbers, and activity coefficients of 1, it is shown in Appendix B that

$$E_{mem} = \frac{2RT}{F} \ln\left(\frac{\frac{C_c^b}{C_d^b} + r_i}{1 - r_i}\right), \tag{11}$$

where R is the gas constant (8.314 J/mol-K) and T [K] is temperature.

Note that once an ED system's architecture (h, ϵ, N, R_{mem}) and its operation (Q) are specified, Eqs. (9)–(11) can be used to compute the voltage V required to operate the stack at a desired current density ratio r_i based on diluate and concentrate conductivity measurements alone. This feature facilitated a straightforward implementation of the model in the experimental feed-forward voltage controller.

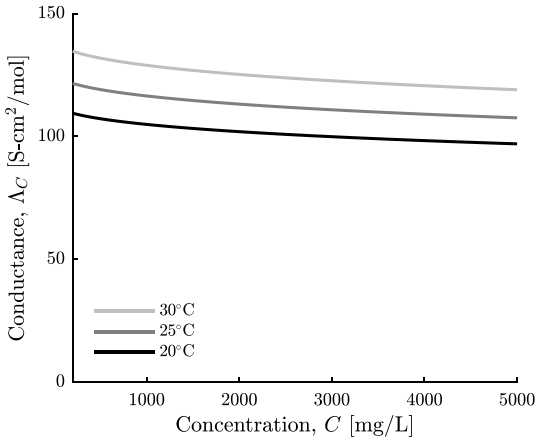

Fig. 5. Equivalent conductance of NaCl solution at varying temperatures, calculated as a function of concentration using the Onsager/Falkenhagen equation with empirical coefficients [43].

In the absence of a concentrate conductivity sensor, the concentrate concentration can be estimated using the mass-balance

$$C_{feed} = C_d^b r + C_c^b (1 - r), \tag{12}$$

where r is the recovery ratio, and the feed concentration is C_{feed}.

Finally, we relate the measured current I [A] to the current density by considering the area that is available for ion-transport,

$$I = i\eta LW, \tag{13}$$

where η represents the open-area fraction of the spacer that occupies the flow channels, and L [m] is the length of the channel (Fig. 1).

3.3. Batch completion time

To derive an analytical prediction for the batch completion time, we neglected the secondary mass-transfer modes of osmosis, back-diffusion, and electroosmosis, and considered only migration. The rate change of concentration in the diluate tank, with volume V_{dil} [m^3], is related to the migration of ions in the ED stack by

$$V_{dil} \frac{dC_d^b}{dt} = -\frac{i\eta LWN}{zF}. \tag{14}$$

Incorporating Eqs. (1) and (8) for the limiting current density and current ratio gives

$$\frac{dC_d^b}{dt} = -\frac{r_i \eta LWNk C_d^b}{V_{dil}(1 - t^{+/-})}. \tag{15}$$

The dilute tank concentration only varies in time during a batch desalination process. Therefore, it is theoretically possible to express any arbitrary function of r_i in time. We can then separate variables and integrate since

$$\int_{C_{feed}}^{C_{prod}} \frac{dC_d^b}{C_d^b} = \int_0^{t_b} -\frac{r_i \eta LWNk}{V_{dil}(1 - t^{+/-})} dt. \tag{16}$$

Therefore,

$$\ln\left(\frac{C_{feed}}{C_{prod}}\right) = \frac{\eta LWNk}{V_{dil}(1 - t^{+/-})} \int_0^{t_b} r_i dt. \tag{17}$$

Introducing a time-averaged current density ratio $\bar{r_i}$ defined as

$$\bar{r_i} = \frac{1}{t_b} \int_0^{t_b} r_i dt, \tag{18}$$

and substituting this definition into Eq. (17) gives our final expression for the batch completion time t_b [s] to desalinate from a given feed concentration C_{feed} to a desired product concentration C_{prod},

$$t_b = \frac{V_{dil}(1 - t^{+/-})}{\bar{r_i} \eta LWNk} \ln\left(\frac{C_{feed}}{C_{prod}}\right). \tag{19}$$

Note that this prediction is expected to be a lower bound on the actual duration since back-diffusion of ions from the concentrate to diluate channels was neglected. Beyond this simplification, we expect this model to be valid for any trajectory of r_i in time, provided that $0 < r_i < 1$.

Table 2
Test stack parameters.

Properties	Values
Number of cell pairs, N	14
Flow path width, W	8 cm
Flow path length, L	8 cm
Channel height, h	0.35 mm
Void fraction, ϵ	0.60 ± 0.04
Open-area fraction, η	0.62 ± 0.04
Cation exchange membranes	PC-SK
Anion exchange membranes	PC-SA

4. Experiments

4.1. Experimental setup

The experimental setup mirrored the schematic in Fig. 3, and was comprised of a PCA GmbH 64-002 ED stack with the construction outlined in Table 2. Geometric parameters were provided by the manufacturer, membrane resistances were determined through system characterization (Appendix A), and the void fraction and spacer open-area fraction were measured in a previous study [34].

Two KNF Flodos NF300 KPDC diaphragm pumps were used to re-circulate the diluate and concentrate through their respective circuits and into separate magnetically-stirred 1 L glass beakers. Flow rates were measured and controlled using two King Instrument 7430 Series glass tube flowmeters with valves (± 6%). To rinse the electrodes, a 0.2 mol/L sodium sulfate solution was circulated at 2.40 ± 0.05 L/min from a separate beaker using a third KNF Flodos NF300 diaphragm pump. All three pumps were powered at a voltage of 23.8 V (± 1%) by a single Mastech HY3003D power supply, which was also used to measure current draw (± 2%).

The conductivities of the diluate and concentrate tanks were measured (± 2%) using Conductivity Instruments CDCE-90 inline conductivity probes, interfacing with CDCN-91 conductivity controllers, with cell constants of K = 1/cm and K = 10/cm, respectively. Conductivity measurements were collected using a National Instruments NI9203 data acquisition module and processed in National Instruments LabVIEW 2018 to calculate, in real-time, the actuation voltage for the voltage-controlled experiments. The computed voltage was then applied (± 0.1%) across the stack using an Agilent Technologies N8760A DC power supply, which also measured current draw (± 0.1%). Diluate and concentrate pH (± 0.01) were recorded at the start and end of each test using a VWR International SympHony H10P handheld meter with a gel-filled pH electrode (89231-608), calibrated using reference solutions of pH 4.00, and 7.00.

Feed-water was prepared by adding sodium-chloride to distilled water with a measured initial conductivity of < 10 μS/cm. Before each test, the diluate and concentrate circuits were repeatedly drained and flushed with distilled water from a common beaker until the conductivity of the water in the channels dropped below 30 μS/cm. The feed water was then separated into two volumes and circulated through the system; 1050 ± 10 mL diluate, and 450 mL ± 10 mL concentrate, providing a recovery of 70 ± 1% for all tests.

4.2. Controller description

To design the feed-forward controller highlighted in Fig. 3, which was implemented in National Instruments LabVIEW 2018, we assumed the following simplifications to the system behavior:

1. The dynamics of the concentration boundary layer were neglected, because it was expected to respond at a characteristic mass-diffusion time scale τ_{diff} that is approximately 840 times shorter (Table 3) than the time scale associated with concentration change in the diluate tank τ_{desal}. Using the ED stack properties in Table 2 and sample operating conditions in Table 3,

$$\tau_{diff} = \frac{l_{BL}^2}{D_{aq}} = \frac{d_h^2}{Sh^2 D_{aq}} \tag{20}$$

since $l_{BL} = \frac{d_h}{Sh}$ is the relevant length-scale, and

$$\tau_{desal} = \frac{V_{dil}(C_{feed} - C_{prod})zF}{i\eta WLN}. \tag{21}$$

2. Spatial concentration variations across the length of the channels within the ED stack were neglected because the residence time of the solution τ_{res} was approximately 180 times smaller than τ_{desal} (Table 3), where

$$\tau_{res} = \frac{L}{u_{ch}}. \tag{22}$$

Alternatively, the maximum change in concentration obtained with a single pass of diluate,

$$\Delta C = \tau_{res}\frac{i\eta}{zF\epsilon h}, \tag{23}$$

was < 28% of the stack inlet concentration C_d^b (for $I < 1$ A), which in turn is assumed equal to the tank concentration at all times.

Table 3
Sample operating conditions, corresponding time scales, and estimated concentration change for the experimental ED stack.

Variables	Values
Flow rate, Q	54 L/h
Resultant linear flow velocity, u_{ch}	0.06 m/s
Diluate tank volume, V_{dil}	1.05 L
Feed concentration, C_{feed}	2000 mg/L
Product concentration, C_{prod}	200 mg/L
Current density, i	250 A/m^2
Current, I	1 A
Diffusion time scale, τ_{diff}	0.3 s
Desalination time scale, τ_{desal}	226 s
Residence time, τ_{res}	1.3 s
Concentration change, ΔC	557 mg/L
Fractional change, $\Delta C/C_{feed}$	28%

Given the two key assumptions above, the simple controller implemented in this study used conductivity measurements, from the diluate and concentrate tanks, to calculate the stack voltage that would produce a desired current density (Fig. 6). The input voltage V control signal was not adjusted based on measurements of the system output, the current I. This subtle distinction explains why the proposed method is classified as a *feed-forward*, and not a *feedback*, control strategy.

The characteristic time scales provided in Table 3 were also used to identify appropriate frequencies for conductivity measurement and voltage actuation. Diluate conductivity was measured at a frequency of 1 Hz, which is greater than the estimated characteristic frequency of change: $1/\tau_{desal} = 0.004$ Hz. We frequently updated the voltage input in response to the changing diluate concentration. However, the corresponding frequency of voltage actuation did not exceed the rate at which the concentration boundary layer redeveloped, nor the rate at which diluate traveled through the system. Hence,

$$\frac{1}{\tau_{diff}} > \frac{1}{\tau_{res}} > \frac{1}{\tau_{act}} > \frac{1}{\tau_{desal}}, \tag{24}$$

where $1/\tau_{act} = 0.1$ Hz. Note that this method of voltage control differs from pulsed-field ED, whereby voltage is actuated at a frequency matching $1/\tau_{diff}$ to perturb the concentration boundary layer within the channels [44,45].

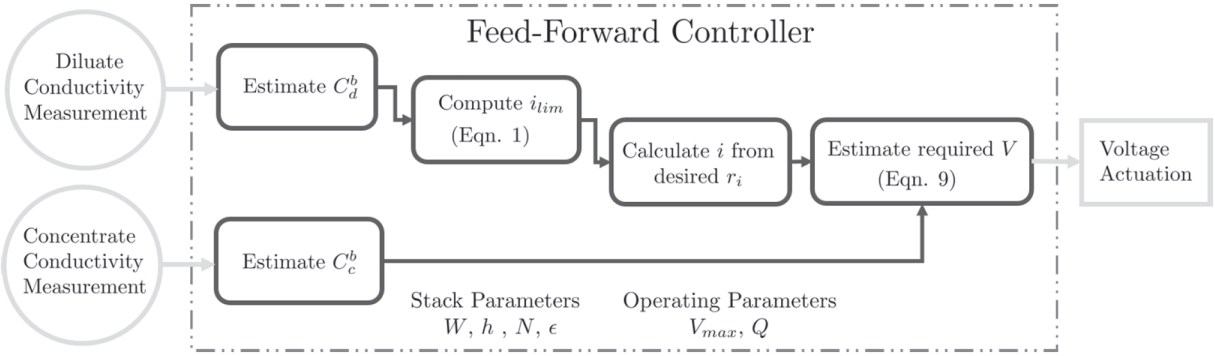

Fig. 6. Flow diagram indicating sensing, controller logic, and actuation for feed-forward voltage-controlled batch. Stack geometry and operating parameters are pre-programmed onto the controller.

4.3. Tests

A summary of the tests conducted in this study is provided in Table 4. Tests 1–5 were baseline conventional constant-voltage batch processes. For the voltage-controlled tests, 6–8, 9–11, and 12–14 systematically investigated the effects of varying the maximum voltage, the current density ratio, and the recirculation flow rates, respectively. The flow rates of 72, 54, and 36 L/h, correspond to linear flow velocities of 8.5, 6.4, and 4.3 cm/s in the channels. Lastly, the limiting current density was intentionally exceeded for Test 15 to examine the effect on pH.

5. Results and discussion

5.1. Current-tracking accuracy

The feed-forward controller was capable of providing the desired current with acceptable performance. The measured current was approximately within −15 to +20% of the current predicted by the model, at the voltages applied through Tests 1–14 (Fig. 7). A comparison for Test 15 is not included because the model is invalid at over-limiting currents.

Table 4
Summary of test parameters.

No.	Operation	Feed concentration C_{feed} (mg/L)	Product concentration C_{prod} (mg/L)	Applied (CV) or Max (VC) Voltage V (V)	Max (CV) or Target (VC) Current density ratio r_i	Flow rate Q [L/h]
1	CV	1500	500	16.7	0.7	54
2	CV	3000	400	12.3	0.6	54
3	CV	2000	300	14.5	0.6	72
4	CV	2000	300	11.6	0.6	54
5	CV	2000	300	10.7	0.6	36
6	VC	1500	500	20.0	0.7	54
7	VC	1500	500	23.0	0.7	54
8	VC	1500	500	26.0	0.7	54
9	VC	3000	400	–	0.4	54
10	VC	3000	400	–	0.6	54
11	VC	3000	400	–	0.8	54
12	VC	2000	300	–	0.6	72
13	VC	2000	300	–	0.6	54
14	VC	2000	300	–	0.6	36
15	CV	3000	400	60	> 1	54

Notes:
• 'CV' refers to constant-voltage, and 'VC' refers to voltage-controlled.
• Applied Voltage for constant-voltage experiments is determined by the limiting current density at C_{prod} and r_i.
• Maximum voltage was not constrained for tests 9–14.

The current-tracking accuracy of the proposed feed-forward controller can be improved by considering the effect of flow rate on stack resistance. The apparent increase in measured current with flow rate (Fig. 7) indicated that the resistance of the ED stack decreases with increasing linear flow velocity. This observation is consistent with the work of Długołecki et al. [46] and Galama et al. [47], who used electrochemical impedance spectroscopy (EIS) to demonstrate that this flow-dependent resistance is associated with the diffusion boundary layers at fluid-membrane interfaces. By adjusting the membrane resistance model to accommodate this phenomenon, the current-draw may be more accurately predicted over a broad range of flow rates. Another possible explanation is that a low flow rate increases the residence time of the solution, producing a large concentration change between the stack inlet and outlet, which consequently increases resistance. For ED stacks consisting of flow paths that are several times longer than those in our experimental bench-scale system, the model recommended in this work may introduce additional errors by neglecting the spatial concentration variations within the stack. Feedback control could also improve current tracking. Here, current measurements would be used to regulate the voltage input to the ED stack.

5.2. pH changes

An acidic shift in the diluate pH is encountered when water-splitting occurs [48,49]. When the stack was intentionally operated above the limiting current density for Test 15, the pH decreased from 6.01 ± 0.02 to 4.65 ± 0.01 (pH data provided as supplementary material). To identify other tests where the limiting current density may have been exceeded, the ratio of the final to initial pH was plotted (Fig. 8).

During all voltage-controlled tests but 11, the pH increased by a similar or greater factor than the corresponding constant-voltage benchmark tests. The pH decrease in Test 11 (pH ratio < 1) signified that voltage-control at the aggressive target current ratio of 0.8 caused the limiting current density to be exceeded. In this work, the limiting current density was calculated using the measured diluate tank (or stack inlet) concentration C_d^b. Combining Eqs. (1), (8), and (23), the fractional concentration change across the stack is approximately

$$\frac{\Delta C}{C_b^d} = \frac{r_i k \eta L}{(1 - t^{+/-})\epsilon h u_{ch}}. \tag{25}$$

Evaluated at a target current ratio of $r_i = 0.8$, and using the geometric and experimental parameters listed in Tables 2 and 4, the concentration decreased by 38% across the stack in Test 11. Consequently, the local limiting current density was proportionally 38% lower at the outlet than at the inlet of the experimental ED stack (Eq. (1)). It follows that we did not provide an appropriate safety-margin against water-splitting for Test 11, because the voltage evaluated for $r_i = 0.8$ at the inlet concentration caused $r_i > 1$ locally at the outlet. Eq. (25) further indicates that longer flow paths will increase the concentration change, thereby decreasing the current ratio that can be safely achieved.

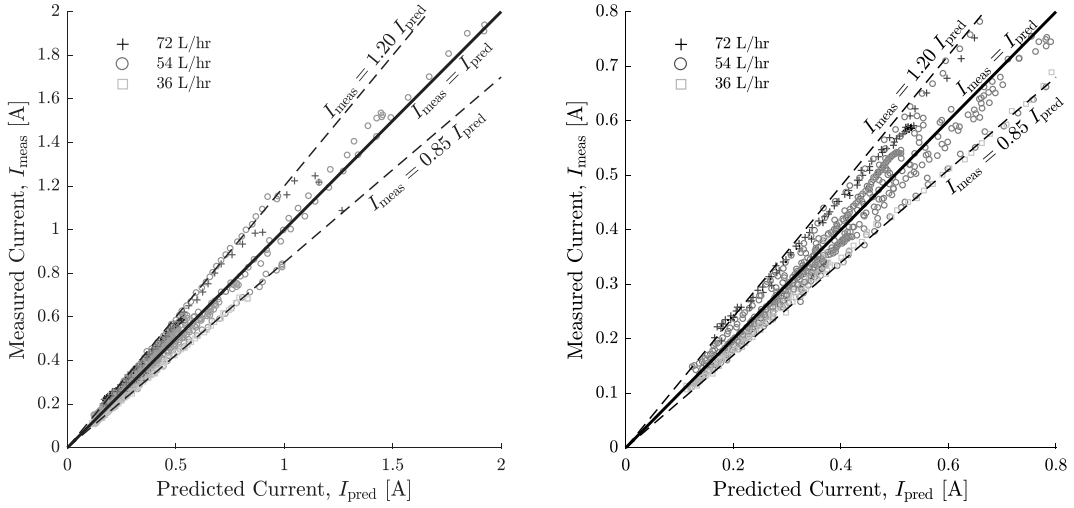

Fig. 7. Measured current I_{meas} was within approximately −15 to +20% of the predicted current I_{pred} at the voltages applied during tests 1–14. Comparison over the full range of measured currents is shown on the *left*, and over the lower (< 0.8 A) range on the *right* for visual clarity.

5.3. The effect of varying current ratio

The total area under the i_{lim} vs. C_b^d curve represents a system's available desalination capacity from a feed to a product concentration (Fig. 4). At higher current density ratios, feed-forward voltage-control captures a larger fraction of this capacity than constant-voltage operation (Fig. 9a). As a direct result, our tests showed that as the target current density ratio was increased from tests 9 through 11, the batch completion time decreased (Fig. 9b).

Measured batch completion times t_b (Table 5) agreed with predictions (Eq. (19)) at the experimental time-averaged current density ratios $\bar{r}_i$. These ratios were computed by dividing the measured current density by the calculated limiting current density (Eq. (1)), and averaging over time. A small but systematic under-prediction of batch completion time was observed, because back-diffusion of ions from the concentrate to the diluate channels was neglected in the analytical prediction (Section 3.3).

At the same 54 L/h flow rate and concentration change of 3000 to 400 mg/L, the constant-voltage process achieved an actual time-averaged current density ratio $\bar{r}_i$ of 0.39 ± 0.01; therefore, the reduction in the batch time of 15 ± 1% observed for Test 9 is explained by the controller exceeding the target r_i of 0.40 during the experiment (Table 5). It is important to note however that while the constant-voltage operation provided a similar *average* current density ratio, the *instantaneous* ratio was lower than 0.40 at the start but approached 0.60 by the end of the batch process. In this specific case then, voltage-controlled desalination at a constant 0.40 current density ratio would provide the same batch completion time as constant-voltage desalination, while decreasing the risk of water splitting.

Increasing the target r_i from 0.4 to 0.6 provided a more substantial decrease in the batch completion time than an equivalent increase from 0.6 to 0.8 (Fig. 9 and Table 5). This observation signifies that the batch completion time decreases at a diminishing rate with increasing current density ratio because from our predictive model (Eq. (19)),

$$t_b \propto \frac{1}{\bar{r}_i}. \tag{26}$$

This result agrees with the work of Min and Kim who also experimentally observed diminishing improvements in the salt removal rate as voltage was increased in their batch desalination trials of groundwater samples [23]. A 61% decrease in the time to achieve 80% chloride ion removal was observed when the applied voltage was raised from 10 to 20 V, but the additional decrease was only 31% when the voltage was again raised by 10 V. Similarly, by raising the applied voltage from 40 to 60 V, Ortiz et al. experimentally measured a 17.9% reduction in the batch processing time of a 2000 mg/L NaCl solution to 500 mg/L [19]. A further increase of 20 V only decreased the processing time by an

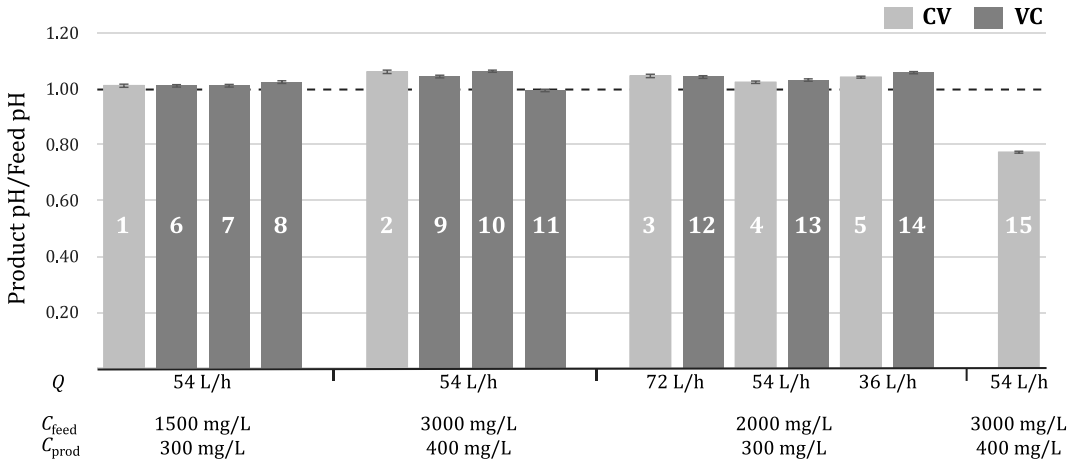

Fig. 8. Ratio of the product pH to feed pH is plotted for both constant-voltage (CV) and voltage-controlled (VC) tests. Tests are first grouped by concentration change, followed by flow rate, and Test 15 represents the case where the limiting current density was deliberately exceeded.

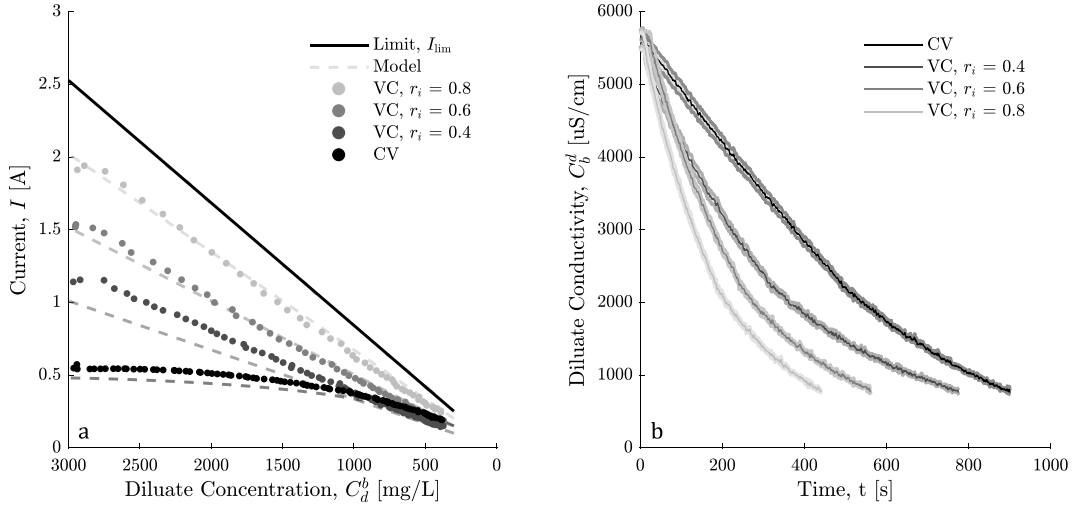

Fig. 9. (a) Current is plotted against diluate concentration for voltage-controlled (VC) and constant-voltage (CV) desalination. Error-bars are smaller than the markers. (b) Diluate conductivity is plotted against time, indicating that as the target current ratio r_i was increased, the time to desalinate 1.05 ± 0.01 L from 1500 mg/L to 500 mg/L decreased. The shaded region represents measurement uncertainty.

Table 5
Summary of batch completion times at varying target current ratios.

Test	Operation	Target r_i	Time-averaged meas $\bar{r}_i$	Pred t_b at $\bar{r}_i$ [s]	Meas t_b [s]
2	CV	–	0.39 ± 0.01	760 ± 95	888 ± 13
9	VC	0.4	0.45 ± 0.02	660 ± 80	752 ± 9
10	VC	0.6	0.57 ± 0.02	520 ± 65	556 ± 6
11	VC	0.8	0.74 ± 0.03	400 ± 50	430 ± 7

additional 11.8%. Note that in both cases, increasing the applied voltage raised the time-averaged current ratio.

From the same predictive model, if the production rate V_{dil}/t_b is held constant, then the total required membrane area scales as

$$NLW \propto \frac{1}{\bar{r}_i}. \tag{27}$$

Hence, reductions in the batch completion time can be alternatively interpreted as membrane-area savings. Therefore, the capital cost of an ED system can be decreased by raising the average current density ratio $\bar{r}_i$ using feed-forward voltage-control.

Having verified the predictive batch completion time model (Eq. (19)) at different r_i, we used it to develop scaling arguments for the pumping and desalination energy consumption. The solutions were circulated at a constant flow rate; hence, the energy consumed by pumping E_p was expected to scale proportionally with batch duration t_b at a constant pumping power, giving

$$E_p \propto \frac{1}{\bar{r}_i}. \tag{28}$$

Extending the circuit analogy for ED (Eq. (9)), the power consumed by ion-transport P_d scales with current squared from Ohm's Law, entailing that

$$P_d \propto \bar{r}_i^{\,2} \tag{29}$$

for a constant membrane area. Multiplying this equation with the scaling relationship for batch duration t_b (Eq. (26)) gives

$$E_d \propto \bar{r}_i, \tag{30}$$

where E_d is the desalination energy consumption.

Experimental measurements of the desalination and pumping energy consumption matched the proposed scaling arguments (Fig. 10). The desalination energy is reported as the numerical integration of the measured ED power in time through the batch cycle, whereas pumping energy is the power-draw of the pumps multiplied by the batch completion time. As shown, voltage-controlled operation decreased the total ($E_d + E_p$) specific energy consumption E_s (Fig. 10) because pumping consumed more energy than desalination for this system. From the scaling trend-lines, the minimum energy consumption is expected at a high average current density ratio of $\bar{r}_i = 0.75$. A higher pump efficiency, wider flow channels, and higher-resistance ion-exchange membranes are all expected to shift this optimal point to lower values of $\bar{r}_i$.

5.4. The effect of varying linear flow velocity

The measured and predicted batch completion times were plotted against linear flow velocity (Fig. 11). The model curves were derived

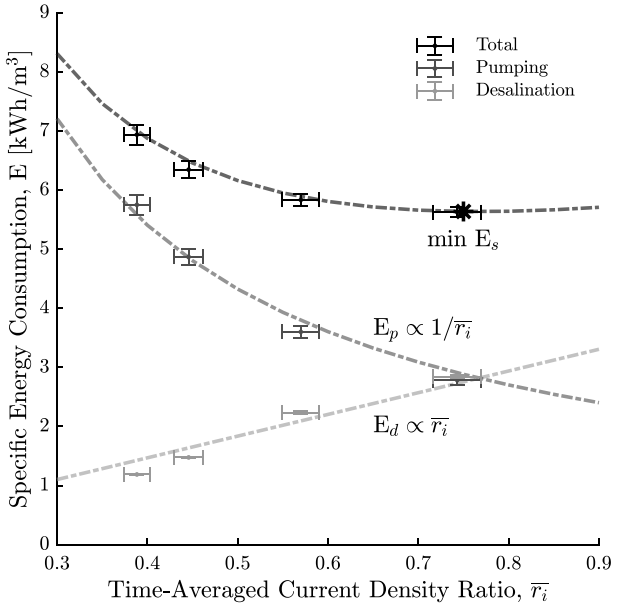

Fig. 10. Increasing the time-averaged current density ratio $\bar{r}_i$ using feed-forward voltage-control decreased total specific energy consumption E_s, by reducing pumping energy consumption E_p. For all cases, the system desalinated 1.05 ± 0.01 L from 3000 mg/L to 400 mg/L, with diluate and concentrate solutions recirculating at 54 L/h.

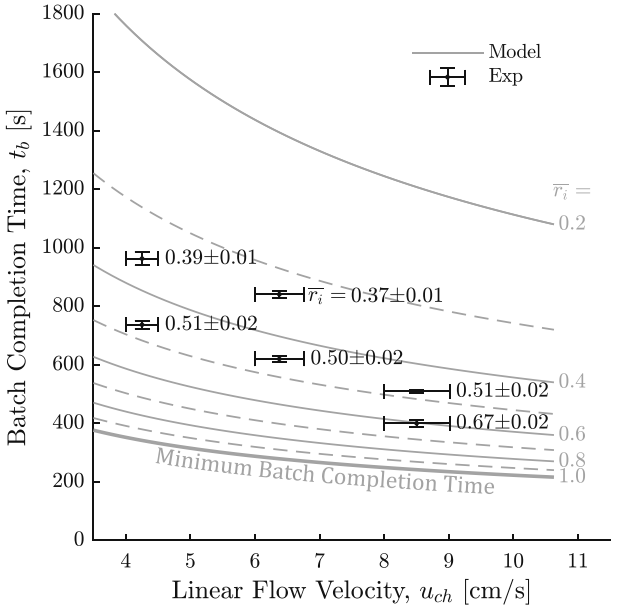

Fig. 11. The measured batch times t_b at varying linear flow velocities and average current density ratios $\bar{r}_i$ agree with model predictions. In all cases, the system desalinated 1.05 ± 0.01 L from 2000 mg/L to 300 mg/L.

using Eq. (5), and the experimental data are labeled with the measured time-averaged current density ratios. Our observations include:

1. The measured batch completion times agree with the model, but are slightly under-predicted. As previously discussed, this small discrepancy is likely explained by back-diffusion of ions from the concentrate to the diluate channels, which lengthens the desalination process.
2. The relative reduction in batch completion time between constant-voltage and voltage-controlled operation (t_b^{VC}/t_b^{CV}) was equal to the inverse fraction of the time-averaged current density ratios ($\bar{r}_i^{CV}/\bar{r}_i^{VC}$), within experimental error at all three flow rates (Table 6). This result further validates the predictive batch time model (Eq. (19)).
3. Irrespective of operation mode (voltage-controlled or constant-voltage), it follows from the item above that increasing $\bar{r}_i$ from one fixed value to another will yield the same *fractional* change in the batch completion time at all flow rates.
4. Any fixed increase in the current density ratio produces a greater *absolute* reduction in batch completion time at lower flow velocities, compared to higher flow velocities. Graphically represented, the difference in t_b at $\bar{r}_i = 0.2$ vs. $\bar{r}_i = 1$ decreases as flow velocity increases (Fig. 11). Therefore, feed-forward voltage-control yields the greatest production and/or cost benefits, relative to constant-voltage operation, at low flow velocities.
5. Shown again here is that increasing $\bar{r}_i$ will provide diminishing returns on production rate (or capital cost), whereby the batch completion time t_b (or total membrane area *NLW*) converges to a velocity dependent theoretical minimum at $\bar{r}_i = 1$.

Table 6
Fractional reduction of batch completion times at varying linear flow velocities.

Velocity, u_{ch} [cm/s]	$\bar{r}_i^{CV}/\bar{r}_i^{VC}$	t_b^{VC}/t_b^{CV}
8.5 ± 0.5	0.77 ± 0.04	0.79 ± 0.03
6.4 ± 0.4	0.74 ± 0.04	0.74 ± 0.02
4.3 ± 0.3	0.76 ± 0.04	0.77 ± 0.02

In addition, Fig. 11 forms a useful tool for designing and analyzing the performance of ED systems. After plotting the measured performance of an existing batch process, it provides a graphical means for determining the maximum possible production rate, and the improvements that can be attained using voltage-control and higher flow velocities.

5.5. The effect of varying maximum voltage

Thus far, we have analyzed the performance of feed-forward voltage-control at varying target current density ratios, with no limitations on stack voltage. Now we assess the behavior at a fixed target current density ratio of $r_i = 0.6$, but impose varying maximum stack voltages (Fig. 12).

Again, the batch completion times for trials 1 and 6–8 matched theoretical predictions within experimental error (Table 7), providing further validation that Eq. (19) is valid for any function of r_i in time. However, in contrast to previous cases, voltage-control did not substantially decrease the batch completion time when compared to constant-voltage operation. In addition, there was no measurable difference in batch completion time as the maximum voltage was varied from 20.0 to 26.0 V. By comparing these results with the other trials conducted at 54 L/h, this behavior was attributed to three factors:

1. From Eq. (19), the batch completion time scales as
$$t_b \propto \ln\left(\frac{C_{feed}}{C_{prod}}\right). \tag{31}$$
As a result, any change in the average current ratio $\bar{r}_i$ will yield a higher reduction in the batch time when desalinating through larger concentration changes. This relationship is graphically represented is Fig. 13, and shown to agree with all trials conducted at 54 L/h.
2. A high average current ratio can be obtained with standard constant-voltage operation when the concentration difference between the feed and product is small, because the 'untapped capacity' in Fig. 4 is narrow. For example, we observed a time-averaged current ratio of 0.57 ± 0.02 when desalinating from 1500 to 500 mg/L in Test 1, whereas this ratio is lower for Tests 2 (3000 to 400 mg/L) and 4 (2000 to 300 mg/L): 0.39 ± 0.01 and 0.37 ± 0.01, respectively. Conversely, when desalinating through large concentration differences, the average current ratio achieved at a constant-voltage is low. Here, small $\bar{r}_i$ changes using feed-forward voltage-control can improve production performance significantly.
3. When plotting current against diluate concentration (Fig. 12a), we observed that increasing the maximum voltage results in significant differences in the current-draw at concentrations exceeding 1000 mg/L. However, the change in diluate concentration from 1500 (2942 μS/cm) to 1000 mg/L (1993 μS/cm) occurs within only ~100 s of the full ~300 s batch duration (Fig. 12a). At concentrations below 1000 mg/L, current differences between the voltage-controlled trials become negligible. Averaging over time then, the overall differences in $\bar{r}_i$ are diminished.

Together, items 1–3 indicated that the highest utility is derived from time-variant voltage-control when producing low-salinity water from highly concentrated feeds.

6. Conclusions

Batch desalination using a single ED stack is implemented when space constraints prohibit continuous desalination using a cascade of ED stages. However, batch desalination is often performed at a constant voltage, causing the membranes to be under-utilized initially during the cycle when higher currents could be sustained. Time-variant, feed-forward voltage-control was investigated as a method to utilize this

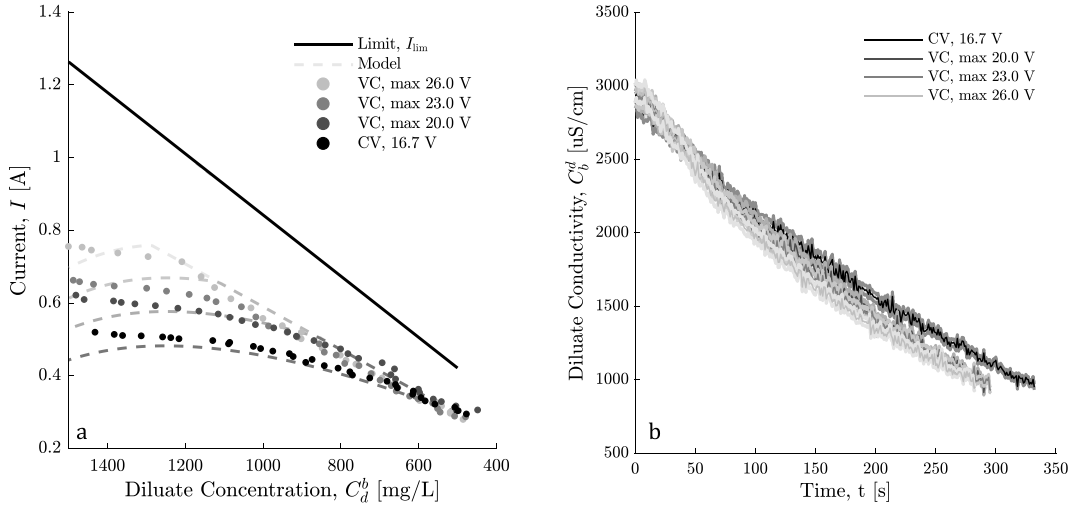

Fig. 12. (a) By raising the maximum voltage allowable for feed-forward voltage-control (VC), a higher initial current was obtained than with constant-voltage desalination (CV). Error-bars are smaller than the markers. (b) Diluate conductivity is plotted against time, indicating that the VC tests desalinated 1.05 ± 0.01 L from 1500 mg/L to 500 mg/L within a similar duration, but all quicker than the CV trial. The shaded region represents measurement uncertainty.

Table 7
Summary of batch completion times at varying maximum voltages.

Test	Max V	Operation	Time-averaged meas $\bar{r}_i$	Pred t_b at $\bar{r}_i$ [s]	Meas t_b [s]
1	16.7	CV	0.57 ± 0.02	283 ± 44	336 ± 19
6	20.0	VC	0.63 ± 0.02	256 ± 39	283 ± 6
7	23.0	VC	0.62 ± 0.02	260 ± 40	277 ± 6
8	26.0	VC	0.65 ± 0.02	248 ± 38	276 ± 6

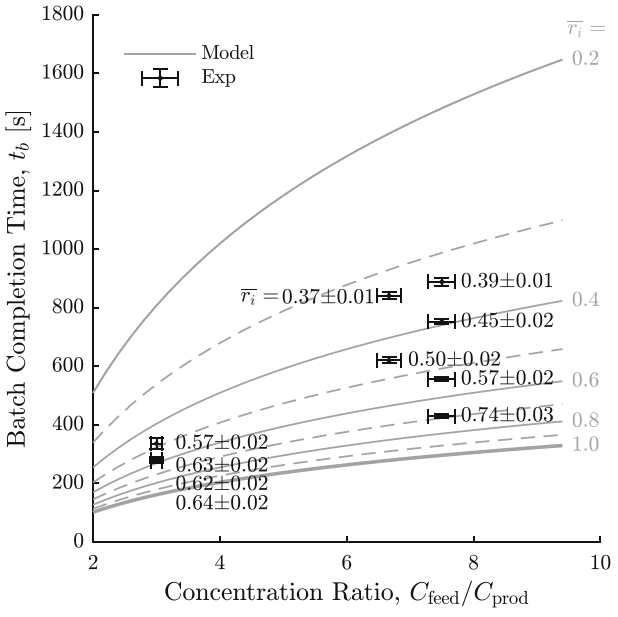

Fig. 13. The measured batch times t_b at varying feed-to-product concentration ratios, and average current density ratios $\bar{r}_i$, agree with model predictions for all trials conducted at a 54 L/h flow rate. As this concentration ratio increases, a larger reduction in batch completion time t_b can be obtained using voltage-control.

unused membrane capacity, and increase production rate or decrease the required membrane area relative to conventional constant-voltage operation. Without affecting pH change, a maximum fractional reduction in batch completion time of 37% ± 2% was experimentally obtained while desalinating from 3000 to 400 mg/L at a linear flow velocity of 6.4 cm/s.

We analytically predicted the batch completion times, and demonstrated close agreement with experimental measurements for varying brackish feeds (1500, 2000, and 3000 mg/L), products (200, 300, and 500 mg/L), linear flow velocities (4.3, 6.4, and 8.5 cm/s), and for both constant-voltage and voltage-controlled desalination. This model indicates that the batch completion time is inversely proportional to the time-averaged ratio of applied to limiting current density. Therefore, voltage-control increased the production rate by achieving higher ratios than is possible with constant-voltage desalination. The largest productivity gains are derived at low flow velocities and high feed-to-product concentration ratios. If pumping consumes more energy than ion-transport, voltage-control was shown to also decrease the total specific energy consumption.

Finally, we designed and experimentally evaluated a feed-forward voltage-controller that can be fitted to a conventional batch ED system without additional sensors. Using diluate and concentrate conductivity measurements, and a simple model of the ED process, the controller tracked the desired current to within −15 to +20%. This performance can be improved by addressing flow velocity effects on diffusion boundary layer resistance, resolving spatial concentration variations across long flow paths, and implementing feedback.

It is our aim that this work will provide designers and operators with both graphical (Fig. 11) and simple analytical tools (Eq. (19)) to design and assess batch ED processes, as well as a method to maximize their systems' production performance. For cost-critical applications such as groundwater desalination in rural communities, we have additionally demonstrated that feed-forward voltage-control is one manner by which drinking water may be more affordably produced.

Acknowledgments

This work was supported by Eureka Forbes Ltd., India, the Tata Center for Technology and Design at MIT, USA, and Tata Projects Ltd., India. Additionally, we acknowledge the support of the Natural Sciences and Engineering Research Council of Canada (NSERC), Canada, funding reference number PGSD3-516795-2018.

Cette recherche a été financé par le Conseil de recherches en sciences naturelles et en génie du Canada (CRSNG), numéro de référence PGSD3-516795-2018.

Appendix A. Empirical R_{mem} model

Constant-voltage experiments spanning the same concentration ranges and flow rates as those in Table 4 were conducted. Membrane resistances were calculated from the applied voltage and measured current, by assuming that the other terms in Eq. (9) were accurately predicted.

Then, using the equation-form recommended by [50], the empirical model of the total (CEM + AEM) membrane resistance was

$$R_{\text{mem}} = A_0 + \frac{A_1}{A_2}\frac{\exp(-A_2 C_d^b) - \exp(-A_2 C_c^b)}{C_c^b - C_d^b}, \tag{1}$$

where A_0, A_1, and A_2 were experimentally-determined coefficients: 0.0046 Ω-m^2, 0.2131 Ω-m^5/mol, and 0.1906 m^3/mol; and C_d^b and C_c^b were the bulk diluate and concentrate concentrations, respectively. Comparison of the model-fit and experimental membrane resistances, which were evaluated as described above, is provided in Fig. A1.

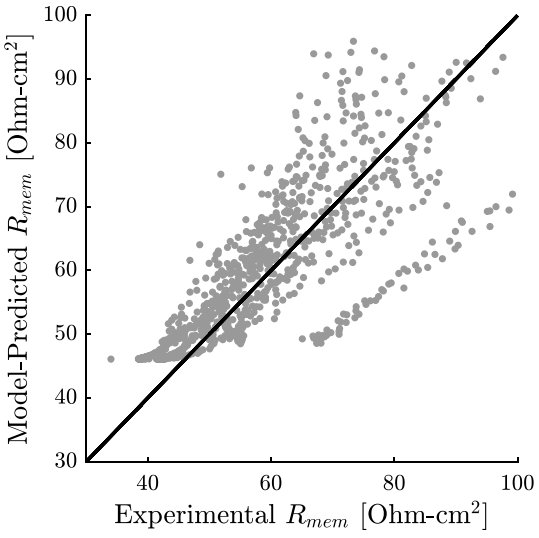

Fig. A1. Model-predicted vs. experimentally derived membrane resistances. The solid line represents a 1:1 relationship.

Appendix B. Derivation of a simplified membrane potential term

A simplified expression for the membrane potential was sought to reduce the real-time computation onboard the voltage-controller. The full expressions for the individual AEM and CEM potentials, taken from previous work [19,34] are

$$E^{AEM} = \frac{(2t^{AEM} - 1)RT}{F}\log\left(\frac{\gamma_c C_c^{AEM}}{\gamma_d C_d^{AEM}}\right)\text{and} \tag{1}$$

$$E^{CEM} = \frac{(2t^{CEM} - 1)RT}{F}\log\left(\frac{\gamma_c C_c^{CEM}}{\gamma_d C_d^{CEM}}\right), \tag{2}$$

where γ is the activity coefficient of the solution and t^{AEM} and t^{CEM} are the apparent transport numbers of the counterions (the anions in the AEM and cations in the CEM, respectively). The wall concentrations C_d^{AEM}, C_d^{CEM}, C_c^{AEM}, and C_c^{CEM} are obtained from balancing the diffusion of ions from the bulk flow to the membrane with migration across it. The individual expressions are

$$C_d^{AEM} = C_d^b - \frac{i(t^{AEM} - t^-)}{zFk}, \tag{3}$$

$$C_d^{CEM} = C_d^b - \frac{i(t^{CEM} - t^+)}{zFk}, \tag{4}$$

$$C_c^{AEM} = C_c^b + \frac{i(t^{AEM} - t^-)}{zFk}, \text{ and} \tag{5}$$

$$C_c^{CEM} = C_c^b + \frac{i(t^{CEM} - t^+)}{zFk}, \tag{6}$$

where C_c^b and C_d^b represent the bulk concentrate and diluate concentration, respectively.

To simplify these terms, we employ the following approximations in this work:

1. Membranes are assumed to be perfectly permselective, so that both t^{AEM} and t^{CEM} equal 1. McGovern et al. measured them to be 0.96 ± 0.04 for concentrations below 10, 000 mg/L [51]; hence, this is an easily justified simplification.
2. The activity coefficients γ_d and γ_c are set to 1. In reality, they are temperature and concentration dependent, but our previous work [34] found that setting them to 1 affects the membrane potential prediction by less than 10% for the concentration ranges investigated in this paper.

Furthermore, since the diluate channels offer the dominant impedance in brackish water desalination, the error introduced by this approximation has an even smaller effect on the voltage calculation (Eq. (9)).

3. For the purposes of estimating the membrane potential, the transport numbers of the cation and anion are both approximated as being equal to the minimum of the actual transport numbers: $t^{+/-} = \min(t^+, t^-)$. This simplification is made so that together with approximation 1, the wall concentrations can be expressed as functions of the limiting current density by substituting Eq. (1) and getting

$$\frac{C_d^{MEM}}{C_d^b} = 1 - \frac{i}{i_{\lim}}, \text{ and} \tag{7}$$

$$\frac{C_c^{MEM}}{C_d^b} = \frac{C_c^b}{C_d^b} + \frac{i}{i_{\lim}}. \tag{8}$$

Note that within each channel, the wall concentrations at both membranes are equal under this approximation. Eqs. (7) and (8) further assume that the mass transfer coefficient k are equal in both the diluate and concentrate channels. This is a reasonable assumption if the channels and flow rates are identical, which is true for conventional ED processes.

Incorporating the above approximations into Eqs. (1) and (2), and summing the two gives the simplified total membrane potential

$$E_{\text{mem}} = \frac{2RT}{F} \ln\left(\frac{\frac{C_c^b}{C_d^b} + r_i}{1 - r_i}\right), \tag{9}$$

where r_i is defined as the ratio $i/i_{\lim}$.

References

[1] N.C. Wright, A.G. Winter V, Justification for community-scale photovoltaic-powered electrodialysis desalination systems for inland rural villages in India, Desalination 352 (2014) 82–91.
[2] H. Strathmann, Electrodialysis, a mature technology with a multitude of new applications, Desalination 264 (3) (2010) 268–288.
[3] Low Energy Solutions for Drinking Water Production by a Revival of Electrodialysis Systems, REvivED Water Consortium, (2016).
[4] A. Campione, L. Gurreri, M. Ciofalo, G. Micale, A. Tamburini, A. Cipollina, Electrodialysis for water desalination: a critical assessment of recent developments on process fundamentals, models and applications, Desalination 434 (October 2017) (2018) 121–160.
[5] J. Schoeman, A. Steyn, M. Makgae, Evaluation of electrodialysis for the treatment of an industrial solid waste leachate, Desalination 186 (1) (2005) 273–289.
[6] A. Elmidaoui, L. Chay, M. Tahaikt, M.M. Sahli, M. Taky, F. Tiyal, A. Khalidi, M.R.A. Hafidi, Demineralisation for beet sugar solutions using an electrodialysis pilot plant to reduce melassigenic ions, Desalination 189 (1) (2006) 209–214.
[7] J.M. Ortiz, E. Expósito, F. Gallud, V. García-García, V. Montiel, V. a. Aldaz, Desalination of underground brackish waters using an electrodialysis system powered directly by photovoltaic energy, Sol. Energy Mater. Sol. Cells 92 (12) (2008) 1677–1688.
[8] Y. Oren, E. Korngold, N. Daltrophe, R. Messalem, Y. Volkman, L. Aronov, M. Weismann, N. Bouriakov, P. Glueckstern, J. Gilron, Pilot studies on high recovery BWRO-EDR for near zero liquid discharge approach, Desalination 261 (3) (2010) 321–330 Special Issue in memory of Sidney Loeb (1917-2008).
[9] R.C. Harries, D. Elyanow, D.N. Heshka, K.L. Fischer, Desalination of brackish groundwater for a prairie community using electrodialysis reversal, Desalination 84 (1-3) (1991) 109–121.
[10] H.J. Lee, F. Sarfert, H. Strathmann, S.H. Moon, Designing of an electrodialysis desalination plant, Desalination 142 (3) (2002) 267–286.
[11] M. Turek, Optimization of electrodialytic desalination in diluted solutions, Desalination 153 (1-3) (2003) 383–387.
[12] P. Tsiakis, L.G. Papageorgiou, Optimal design of an electrodialysis brackish water desalination plant, Desalination 173 (2) (2005) 173–186.
[13] F.S. Rohman, N. Aziz, Optimization of batch electrodialysis for hydrochloric acid recovery using orthogonal collocation method, Desalination 275 (1-3) (2011) 37–49.
[14] R.K. McGovern, S.M. Zubair, J.H. Lienhard V, Design and optimization of hybrid ED-RO systems for the treatment of highly saline brines, International Desalination Association World Congress, Tianjin, China, 2013.
[15] K.M. Chehayeb, D.M. Farhat, K.G. Nayar, J.H. Lienhard, Optimal design and operation of electrodialysis for brackish-water desalination and for high-salinity brine concentration, Desalination 420 (June) (2017) 167–182.
[16] S.R. Shah, N.C. Wright, P.A. Nepsky, A.G. Winter, Cost-optimal design of a batch electrodialysis system for domestic desalination of brackish groundwater, Desalination 443 (Oct. 2018) 198–211.
[17] K.M. Chehayeb, K.G. Nayar, J.H. Lienhard, On the merits of using multi-stage and counterflow electrodialysis for reduced energy consumption, Desalination 439 (December 2017) (2018) 1–16.
[18] B.A. Qureshi, S.M. Zubair, Design of electrodialysis desalination plants by considering dimensionless groups and variable equivalent conductivity, Desalination 430 (October 2017) (2018) 197–207.
[19] J.M. Ortiz, J.A. Sotoca, E. Expósito, F. Gallud, V. García-García, V. Montiel, A. Aldaz, Brackish water desalination by electrodialysis: batch recirculation operation modeling, J. Membr. Sci. 252 (1-2) (2005) 65–75.
[20] Y. Tanaka, A computer simulation of batch ion exchange membrane electrodialysis for desalination of saline water, Desalination 249 (3) (2009) 1039–1047.
[21] J. Uche, F. Círez, A.A. Bayod, A. Martínez, On-grid and off-grid batch-ED (electrodialysis) process: simulation and experimental tests, Energy 57 (2013) 44–54.
[22] L.J. Banasiak, T.W. Kruttschnitt, A.I. Schäfer, Desalination using electrodialysis as a function of voltage and salt concentration, Desalination 205 (1-3) (2007) 38–46.
[23] J.-H. Min, H.-S. Kim, Effect of operating conditions on the treatment of brackish groundwater by electrodialysis, Desalin. Water Treat. 51 (2013) 5132–5137.
[24] K.G. Nayar, P. Sundararaman, J.D. Schacherl, C.L. O'Connor, M.L. Heath, M.O. Gabriel, S.R. Shah, N.C. Wright, A.G. Winter V, Feasibility study of an electrodialysis system for in-home water desalination in urban India, Dev. Eng. 2 (2016) 38–46.
[25] D.W. Bian, S.M. Watson, N.C. Wright, S.R. Shah, T. Buonassisi, D. Ramanujan, I.M. Peters, A.G. Winter V, Optimization and design of a low-cost, village-scale, photovoltaic-powered, electrodialysis reversal desalination system for rural India, Desalination Under Review (2018).
[26] S.J. Parulekar, Optimal current and voltage trajectories for minimum energy consumption in batch electrodialysis, J. Membr. Sci. 148 (1) (1998) 91–103.
[27] F.B. Leitz, Chapter 2.7 measurements and control in electrodialysis, Desalination 59 (C) (1986) 381–401.
[28] L. Orlovskaja, N. Periene, M. Kurtinaitiene, S. Surviliene, Nisic composite plated under a modulated current, Surf. Coat. Technol. 111 (2) (1999) 234–239.
[29] C. Miller, M. Sarret, T. Andreu, ZnMn alloys obtained using pulse, reverse and superimposed current modulations, Electrochim. Acta 48 (17) (2003) 2397–2404.
[30] A. Chávez-Valdez, A.R. Boccaccini, Innovations in electrophoretic deposition: alternating current and pulsed direct current methods, Electrochim. Acta 65 (2012) 70–89.
[31] B. Lu, Y. Zhao, Y. Song, J. Zhang, Stress-limited fast charging methods with time-varying current in lithium-ion batteries, Electrochim. Acta 288 (2018) 144–152.
[32] M. Panizza, A. Kapalka, C. Comninellis, Oxidation of organic pollutants on BDD anodes using modulated current electrolysis, Electrochim. Acta 53 (5) (2008) 2289–2295.
[33] M.S. Isaacson, A.A. Sonin, Sherwood number and friction factor correlations for electrodialysis systems, with application to process optimization, Ind. Eng. Chem. Process Des. Dev. 15 (1976) 313–321.
[34] N. Wright, S. Shah, S. Amrose, A. Winter V, A robust model of brackish water electrodialysis desalination with experimental comparison at different size scales, Desalination 443 (2018).
[35] S. Pawlowski, J.G. Crespo, S. Velizarov, Pressure drop in reverse electrodialysis: experimental and modeling studies for stacks with variable number of cell pairs, J. Membr. Sci. 462 (2014) 96–111.
[36] A.M. Peers, General discussions, Discuss. Faraday Soc. 21 (1956) 124.
[37] A. Nakayama, Y. Sano, X. Bai, K. Tado, A boundary layer analysis for determination of the limiting current density in an electrodialysis desalination, Desalination 404 (2017) 41–49.
[38] V. Geraldes, M.D. Afonso, Limiting current density in the electrodialysis of multi-ionic solutions, J. Membr. Sci. 360 (1) (2010) 499–508.
[39] S. Pawlowski, P. Sistat, J.G. Crespo, S. Velizarov, Mass transfer in reverse electrodialysis: flow entrance effects and diffusion boundary layer thickness, J. Membr.

Sci. 471 (2014) 72–83.
[40] R. Allgood, A. Gordon, The variation of the transference numbers of sodium chloride in aqueous solution with temperature, J. Chem. Phys. 10 (1942) 124–126.
[41] R. Stokes, The diffusion coefficients of eight uni-univalent electrolytes in aqueous solution at 25 °C, J. Am. Chem. Soc. 72 (5) (1950) 2243–2247.
[42] H. Ozbek, J. Fair, S. Phillips, Viscosity Of Aqueous Sodium Chloride Solutions From 0 - 150C, Lawrence Berkley Laboratory, University of California, Berkeley, California, 1977.
[43] G. Kortüm, Treatise on Electrochemistry, Elsevier Publishing Company, 1965.
[44] P. Sistat, P. Huguet, B. Ruiz, G. Pourcelly, S. Mareev, V. Nikonenko, Effect of pulsed electric field on electrodialysis of a NaCl solution in sub-limiting current regime, Electrochimica Acta 164 (May, 2015) 267–280.
[45] N. Cifuentes-Araya, G. Pourcelly, L. Bazinet, Impact of pulsed electric field on electrodialysis process performance and membrane fouling during consecutive demineralization of a model salt solution containing a high magnesium/calcium ratio, J. Colloid Interface Sci. 361 (1) (2011) 79–89.
[46] P. Długołecki, P. Ogonowski, S.J. Metz, M. Saakes, K. Nijmeijer, M. Wessling, On the resistances of membrane, diffusion boundary layer and double layer in ion exchange membrane transport, J. Membr. Sci. 349 (1-2) (2010) 369–379.
[47] A.H. Galama, D.A. Vermaas, J. Veerman, M. Saakes, H.H. Rijnaarts, J.W. Post, K. Nijmeijer, Membrane resistance: the effect of salinity gradients over a cation exchange membrane, J. Membr. Sci. 467 (2014) 279–291.
[48] V.V. Nikonenko, A.V. Kovalenko, M.K. Urtenov, N.D. Pismenskaya, J. Han, P. Sistat, G. Pourcelly, Desalination at overlimiting currents: state-of-the-art and perspectives, Desalination 342 (2014) 85–106.
[49] M. Andreeva, V. Gil, N. Pismenskaya, L. Dammak, N. Kononenko, C. Larchet, D. Grande, V. Nikonenko, Mitigation of membrane scaling in electrodialysis by electroconvection enhancement, pH adjustment and pulsed electric field application, J. Membr. Sci. 549 (2018) 129–140.
[50] J. Veerman, M. Saakes, S.J. Metz, G.J. Harmsen, Reverse electrodialysis: performance of a stack with 50 cells on the mixing of sea and river water, J. Membr. Sci. 327 (1-2) (2009) 136–144.
[51] R.K. McGovern, A.M. Weiner, L. Sun, C.G. Chambers, S.M. Zubair, J.H. Lienhard V, On the cost of electrodialysis for the desalination of high salinity feeds, Appl. Energy 136 (2014) 649–661.